Research Updates

High-temperature metallic glasses: Status, needs, and opportunities

Jerry Howard,[1] Krista Carlson,[1] and Dev Chidambaram[2,*]

[1]*Department of Materials Science and Engineering, The University of Utah, Salt Lake City, Utah 84112, USA*

[2]*Department of Chemical & Materials Engineering, University of Nevada Reno, Reno, Nevada 89557-0388, USA*

(Received 18 October 2020; revised 8 January 2021; accepted 16 March 2021; published 23 April 2021)

Metallic glasses have drawn the attention of researchers due to their high strength, hardness, high corrosion, and wear resistance, and ease of thermoplastic forming compared to their counterpart crystalline alloys. While these characteristics are desirable for materials used in extreme environments that often need high corrosion resistance and mechanical strength at elevated temperatures, metallic glasses have found limited use because they crystallize at lower temperatures than the operational temperatures of these applications. Upon crystallization, these characteristics are lost. In recent years, refractory metallic glasses with higher crystallization temperatures have been synthesized, making them potential candidates for use in extreme environments, such as in space and nuclear applications. This review summarizes recently reported metallic glass systems with crystallization temperatures above 700 °C. These systems are discussed in terms of glass forming ability, mechanical properties, and other properties relevant to their use in high temperature applications. This article highlights the challenges in the development and implementation of high-temperature metallic glasses, and discusses the needs and research opportunities that exist for expanding our knowledge of these glasses, including potential routes for improving glass forming ability and mechanical properties.

DOI: 10.1103/PhysRevMaterials.5.040301

I. INTRODUCTION

For high temperature applications, a major drawback of traditional metallic glasses (MGs) is that they crystallize at relatively low temperatures below the melting point of an equivalent crystalline alloy. Upon crystallization, the beneficial properties of the glassy state are lost [1]. These properties, which include high strength, high corrosion resistance, high wear resistance [2,3], and high formability through thermoplastic forming, are useful for many applications. Designing MGs with high thermal stability is required for implementation in a wide range of extreme environments [4–6].

Such extreme environments in which high temperature metallic glasses (HTMGs) might be utilized are found in many industries, including military, space travel, and energy production. For example, nuclear energy production presents several highly corrosive, high temperature environments such as molten salts and supercritical water [7,8]. The authors have previously reported on the corrosion behavior of traditional steels and other alloys in molten salts [9,10]. In LiCl-Li_2O molten salts, the presence of Li metal has been shown to degrade metals rapidly as corrosive attack by Li occurs through the grain boundaries [11]. As MGs lack grain boundaries, they are a promising material for this application if compositions which can withstand the high temperatures (typically >700 °C) can be produced [9,12].

MGs are similarly useful in applications in which parts with complex shapes must be made as light as possible, such as aeronautical and space travel applications. As weight savings equate directly to fuel and cost savings in these applications, materials must be capable of forming thin, lightweight parts with high strengths [13]. W alloys are typically used in such applications when extreme temperatures are involved due to their high melting points and high hardness and wear resistance [14]. Due to the low ductility of W, manufacturing W-alloy parts with complex shapes and thin walls is notoriously difficult [15]. In addition, W has a high thermal conductivity, which can be a disadvantage for shaping the metal through additive manufacturing techniques and for applications in which thermal insulation is desired [14,16]. As described below, MGs would possess useful properties for such applications, provided compositions with suitable high temperature stability can be discovered and synthesized.

HTMGs present several advantages over traditional crystalline alloys depending on the application such as higher strength to weight ratio [17], improved corrosion resistance [18], and lower thermal conductivity [19]. MGs have extremely high mechanical strengths which approach theoretical values [20]. This makes them good candidates for applications in which high strength to weight ratio is needed [21]. The high strength of MGs stems from the lack of crystallinity; flaws that typically lead to failure in crystalline alloys (e.g., grain boundaries, dislocations) are absent in glasses [22,23].

MGs are often reported to have improved corrosion resistance over crystalline alloys of the same composition [24–26]. Grain boundaries, dislocations, and chemical inhomogeneities can act as galvanic couples and provide excellent starting points for corrosive attack [27]. MGs are thought to avoid these issues in that they are free of any crystalline structure. With the absence of crystallinity and its accompanying defects, glasses typically display lower rates of corrosion

*dcc@unr.edu

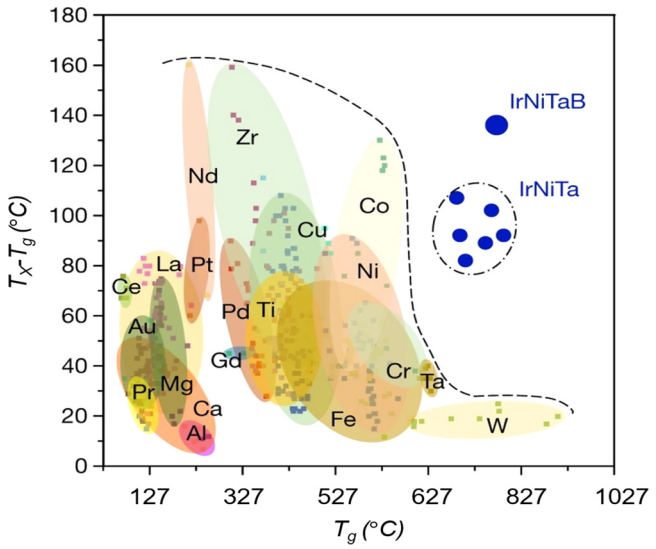

FIG. 1. Strength versus temperature for Ir-Ni-Ta high-temperature BMGs, as well as a variety of alloy classes, including high temperature alloys; high entropy alloys; and Au-, Zr-, and Co-based bulk metallic glasses (BMGs). Reprinted from Ref. [75] with permission from Springer. Temperatures on the x axis have been converted from K to °C.

[28,29]. The excellent corrosion resistance of MGs has also been attributed to the higher reactivity of the glassy phase, which causes a protective film to be formed more quickly and with lower defect density [26,30]. Combined with the greater homogeneity of the glass, this passivating film is often smoother and more protective than in crystalline alloys [28]. This is important as high reactivity is only advantageous for corrosion resistance if a nonporous and structurally robust barrier is formed [26,31]. Some studies have found that the noncrystalline structures of certain compositions did not impart appreciably better corrosion resistance than their crystalline counterparts [32,33]. In these cases, a metallic glass may still be advantageous for corrosion resistance because passivating alloying elements can be added to solid solution beyond conventional limits [34].

High or low values of thermal conductivity can be advantageous depending on the applications. In general, the thermal conductivity of MGs is lower than that of their crystalline counterparts [35–37], stemming from the lack of long-range order in the glassy structure. Atomic disorder increases the difficulty for phonons to transfer heat throughout the material [38]. While low thermal conductivity is beneficial for the applications mentioned above, it may not be desirable for some applications such as electronics [39] or when used as a tool material for drilling and other similar applications [40].

Relatively few MGs reported to date have an onset crystallization temperature (T_x) suitable for use in high-temperature environments like those discussed above. In examining the literature of the past 10 years, over 100 articles referencing MGs with T_x above 600 °C were found. Above 700 °C, only 25 articles involving MGs from the past 10 years were found. After studying Fig. 1 is clear that the majority of MGs have T_x lower than 700 °C, and very few have a glass transition temperature (T_g) above 723 °C. Of the alloys with T_x above 700 °C, a refractory metal is typically the primary component due to the fact that the T_g and T_x of a given MG generally scale with the melting point of the primary constituent [41,42]. The addition of high melting point elements has been shown to increase T_x, thus increasing the range of temperatures at which metallic glasses maintain their unique properties [1,41].

The major shortcoming of refractory metal based MGs is the typically low glass forming ability (GFA) due to high ($\geqslant$1000 °C) liquidus temperatures. GFA is often estimated using the critical casting thickness (d_c) [43]. As the value of d_c is dependent upon the fabrication method, it is not a reliable parameter for estimating GFA. Instead, expressions based on temperature relationships between important glass temperatures—T_g, T_x, T_l (liquidus temperature)—are used to define the criteria. For example, ΔT_x, defined as $T_x - T_g$ (i.e., the supercooled liquid region) is used as an indicator of liquid phase stability. An alloy with high liquid phase stability will more easily bypass crystallization and form a glass. While useful in assessing the suitability of an alloy for thermoplastic forming [44], this criterion has a shortcoming in that GFA cannot typically be attributed to liquid phase stability alone [45]. To overcome this issue, other criteria have been developed, such as $T_{rg}(= T_g/T_l)$ and $\gamma[= T_x/(T_g + T_l)]$ [46]. Both of these commonly used criteria have been successful at predicting GFA. The γ criterion is more comprehensive as it reflects the three aspects attributed to good GFA (liquid phase stability, stability of the supercool liquid, and resistance to crystallization). High GFA results in larger d_c and lower required cooling rates for glass formation [47]. T_{rg} and γ for good glass forming alloys are on the order of 0.500–1.000 [46,47] In regard to HTMGs, which display high liquidus temperatures, the GFA is low, resulting in d_c on the order of 20–50 μm, limiting the usefulness of refractory-based MGs in structural and other industrial applications [1,41]. Studies are still ongoing in the attempt to identify a criterion that can be used unambiguously to index the GFA of MGs.

Of important note when discussing metallic glasses is the difference between a *metallic glass* and an *amorphous metal*. While the two terms are often used interchangeably in the literature, it is worthwhile to differentiate them. In this article, the term metallic glass refers only to materials which are x-ray amorphous and which also exhibit the glass transition phenomenon [48,49]. The glass transition is a phenomenon unique to glasses in which they reversibly and continuously transition from a solid to a supercooled liquid without crystallization [50]. In application, the glass transition is responsible for the unique formability of glasses. The glass transition phenomenon enables thermoplastic forming techniques, such as blow molding, which has been successfully used to produce complex MG parts. Amorphous metals have a noncrystalline structure but do not experience a glass transition. Therefore, amorphous metals cannot be thermoplastically formed to create complex shapes.

The objective of this review article is to examine the literature for factors influencing GFA in HTMGs, as well as their thermodynamic and mechanical properties. This review focuses on these properties because they are the most reported. The HTMGs described in this article are metallic glasses which exhibit T_x values >700 °C. The literature presented in this review is organized based on the highest value of

TABLE I. Selected thermal properties of metallic glasses with crystallization temperatures (T_x) between 700 °C and 749 °C. d_c = critical casting thickness, T_g = glass transition temperature, ΔT_x = supercooled liquid region, T_{rg} = reduced glass transition temperature (T_g/T_l), and $\gamma = T_x/(T_g + T_l)$. MS = melt spinning; SC = copper-mold suction casting.

Composition	d_c (mm)	T_g (°C)	T_x (°C)	ΔT_x (°C)	T_{rg}	γ	Formation method	Reference
$Co_{42}Ir_{15}Ta_8B_{35}$	3	652	709	57	0.615	0.404	MS	[51]
$Co_{47}Ir_{10}Ta_8B_{35}$	5	656	720	64	0.636	0.415	MS	[51]
$Co_{52}Ir_5Ta_8B_{35}$	3	668	729	61	0.641	0.416	MS	[51]
$Co_{57}Ta_8B_{35}$	2	676	728	52	0.636	0.41	MS	[51]
$Fe_{68}Nb_4Y_6B_{22}$	5	594	732	138	–	–	MS	[53]
$Fe_{62}Cr_6Nb_4Y_6B_{22}$	4	603	719	116	–	–	MS	[53]
$Ni_{62}Nb_{13}Ta_{25}$	2	687	733.2	46	0.5931	0.39	SC	[56]
$Ni_{62}Nb_{18}Ta_{20}$	2	675	721.5	46.3	0.5979	0.392	SC	[56]
$Ni_{62}Nb_{23}Ta_{15}$	2	667	706.8	39.8	0.618	0.398	SC	[56]
$Co_{57}Ni_2Ta_6B_{35}$	1.5	667	707	40	0.649	0.41	MS, SC	[63]

T_x in the alloy system. The ranges used are 700 °C–749 °C, 750 °C–799 °C, and ⩾800 °C. HTMGs are discussed in terms of the formation methods used, the GFA, and thermodynamic properties; and mechanical properties, including elasticity, strength, ductility, hardness, and wear resistance. Finally, the literature has been critically examined to determine which areas of study have thus far been neglected, which focuses on corrosion resistance and high temperature mechanical properties.

II. T_x BETWEEN 700 °C AND 749 °C

The thermal properties of glass forming alloys with T_x between 700 °C and 749 °C are presented in Table I. The mechanical properties of the same alloys are presented in Table II. $Co_{57-x}Ir_xTa_8B_{35}$ ($x = 0$, 5, 10, 15) alloys were studied by Wang *et al.* [51]. Ribbon samples were formed through single-roller melt spinning and cylindrical samples were created using injection casting into copper molds. The authors found that the addition of Ir from 0 to 10 at. % improved GFA with d_c increasing from 2 to 5 mm. However, additional Ir (15 at. %) caused the d_c to decrease to 3 mm. In this system, ΔT_x was a good predictor of GFA; ΔT_x changes as a result of Ir concentration corresponded to changes in experimentally determined d_c. T_{rg} and γ were not found to accurately predict the GFA of this system with values of both parameters remaining relatively constant with Ir content variation. Wang *et al.* attributed the increase in GFA to an increase in liquid stability caused by Ir addition. The increase in stability could partially be explained by a higher degree of topological and chemical short-range order with the addition of Ir, which lowered the entropy of the supercooled liquid and, therefore, lowered the thermodynamic driving force for crystallization. The addition of Ir to these MGs also improved plasticity from 0.9% to 1.2% and was likely related to the decrease in T_g. As discussed by Zhang *et al.* [52], T_g is dominated by the bonding forces between the constituent elements and, as a result, it can be used as a macroscopic indicator of changes in plasticity induced by compositional changes. Wang *et al.* also suggested that the high strength values in the CoIrTaB alloys were related to strong bonding forces [51]. During tensile testing at room temperature, the $Co_{47}Ir_{10}Ta_8B_{35}$ specimen split into small fragments. Upon examination of the fragments, vein- and cleavagelike patterns were observed (Fig. 2). It was determined that fracture in this alloy system involved competition between shear and fragmentation modes.

Zhang *et al.* [53] produced HTMGs in the system $Fe_{68-x}Cr_xNb_4Y_6B_{22}$ ($x = 2$–6) by melt spinning and by injection into copper molds. While this study was mainly focused on the magnetic properties of the alloys, the study showed that the GFA decreased when 6% Cr was substituted for Fe. While this substitution increased the number of components in the alloy and would have been expected to increase GFA, the decrease in GFA was explained by the heat of mixing. Cr has

TABLE II. Selected mechanical properties of metallic glasses with crystallization temperatures (T_x) between 700 °C and 749 °C. H_v = Vickers microhardness, E = modulus of elasticity, σ_y = yield strength, σ_f = fracture strength, and ε_p = plastic strain limit.

Composition	H_v (GPa)	E (GPa)	H_v/E	$H_v^2/2E$ (GPa)	σ_y (GPa)	σ_f (GPa)	ε_p (%)	Reference
$Co_{42}Ir_{15}Ta_8B_{35}$	–	–	–	–	–	–	–	[51]
$Co_{47}Ir_{10}Ta_8B_{35}$	–	–	–	–	5.515	5.875	1.1	[51]
$Co_{52}Ir_5Ta_8B_{35}$	–	–	–	–	5.200	5.600	0.9	[51]
$Co_{57}Ta_8B_{35}$	–	–	–	–	–	–	–	[51]
$Fe_{68}Nb_4Y_6B_{22}$	–	–	–	–	–	–	–	[53]
$Fe_{62}Cr_6Nb_4Y_6B_{22}$	–	–	–	–	–	–	–	[53]
$Ni_{62}Nb_{13}Ta_{25}$	–	–	–	–	–	3.291	0.20	[56]
$Ni_{62}Nb_{18}Ta_{20}$	–	–	–	–	–	3.200	1.36	[56]
$Ni_{62}Nb_{23}Ta_{15}$	–	169.4	–	–	–	3.100	1.41	[56]
$Co_{57}Ni_2Ta_6B_{35}$	13.83	–	–	–	5.48	5.63	1.2	[63]

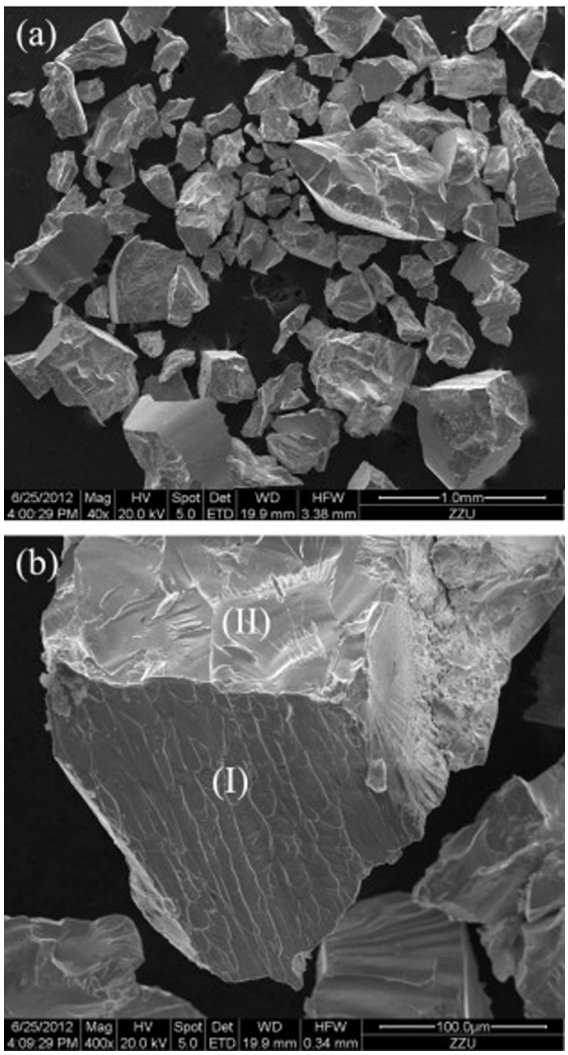

FIG. 2. Scanning electron microscope (SEM) images of $Co_{47}Ir_{10}Ta_8B_{35}$ MG after fracture: (a) fracture fragments and (b) the surface morphology of a fracture fragment. Veinlike patterns seen on the surface at (I) are indicative of shear fragmentation mode. Reprinted from Ref. [51] with permission from Elsevier.

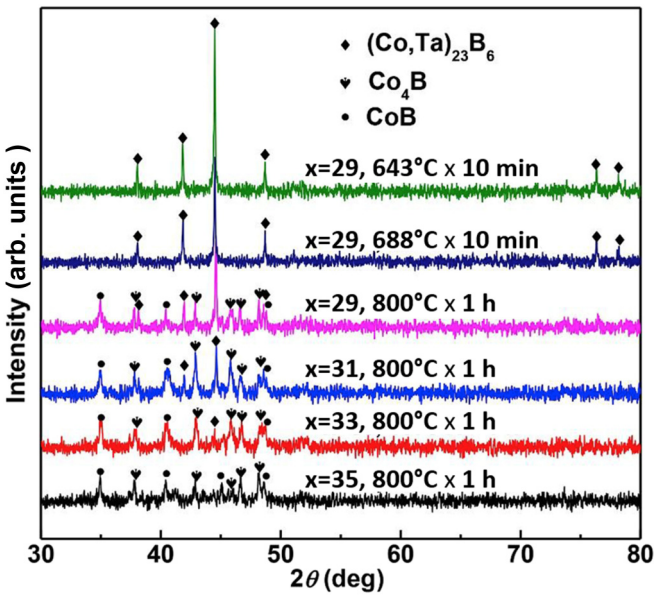

FIG. 3. XRD patterns of annealed $Co_{92-x}Ni_2Ta_6B_x$ ($x = 35$, 33, 31, 29) ribbons. Samples with lower B content form the complex $(Co, Ta)_{23}B_6$ phase while samples with higher amounts of B form two phases that mutually inhibit each other's formation—Co_4B and CoB. Adapted from Ref. [63] with permission from Elsevier. Temperatures have been converted from K to °C.

a less negative heat of mixing with respect to Nb and Y than does Fe, which increased the thermodynamic driving force for crystallization. Mechanical property measurements were not reported.

Binary NiNb alloys have been investigated by several research groups [54–56]. He *et al.* [56] found that the addition of up to 15 at. % Ta to NiNb HTMG alloys increased the parameters associated with GFA. All samples were made with a cylindrical diameter of 2 mm. Both T_{rg} and γ showed a slight increase from 0.6157 and 0.394 to 0.618 and 0.398, respectively. Above 15 at. % Ta, T_{rg} and γ both decreased, indicating a decrease in GFA. Crystallization occurred at above 30 at. % Ta. HTMGs in this study were produced via suction casting into water-cooled copper molds. As may be expected for a refractory metal, increasing Ta content increased all characteristic temperatures. Ta addition also increased strength over binary NiNb alloys [57] with reported strengths being higher than many other previously reported glassy alloys based on NiNb [58–62]. A nearly linear relationship between T_g and fracture strength was observed, as increasing Ta content correlated with increases in both T_g and fracture strength. Following a similar trend to the GFA parameters, the plastic strain increased from 0.76% to 1.41% upon the addition of 15 at. % Ta and decreased above 15 at. %. While typical glassy NiNb alloys show an increase in strength and decrease in plasticity upon replacement of Ni and Nb with Ta, the $Ni_{62}Nb_{23}Ta_{15}$ and $Ni_{62}Nb_{18}Ta_{20}$ reported in this study showed a combination of high strength and relatively high plasticity. The authors attributed the achieved combination of strength and plasticity to the formation of Ta-rich clusters, which changed the thermal stability of the alloy. The small change in composition of the clusters was thought to have acted as nucleation sites for crystals when Ta content reached 30 at. %.

In a study by Zhang *et al.* [63], $Co_{92-x}Ni_2Ta_6B_x$ ($x = 29$, 31, 33, 35) HTMGs were fabricated by both melt-spinning and copper-mold casting methods. Good GFA was exhibited in this system at all compositional values with T_{rg} and γ values as high as 0.651 and 0.410, respectively. The crystallization behavior of the alloys shed light on the mechanisms responsible for giving the alloys their high GFA. At low B levels, $(Co, Fe, Ni)_{23}B_6$ was the favored crystalline phase. The formation of this phase is well known to require long-range atomic rearrangement and, thus, leads to higher supercooled liquid stability and higher GFA. With higher amounts of B, simpler crystalline phases are favored (CoB, Co_4B), which would ordinarily lead to lower GFA. However, these two simple phases are equally in competition in this alloy and mutually inhibit each other's formation, leading to high supercooled liquid stability and high GFA. X-ray diffraction (XRD) patterns of the annealed MG samples are shown in Fig. 3.

TABLE III. Selected thermal properties of metallic glasses with crystallization temperatures (T_x) between 750 °C and 799 °C. d_c = critical casting thickness, T_g = glass transition temperature, ΔT_x = supercooled liquid region, T_{rg} = reduced glass transition temperature (T_g/T_l), and $\gamma = T_x/(T_g + T_l)$. MS = melt spinning; SC = copper-mold suction casting.

Composition	d_c (mm)	T_g (°C)	T_x (°C)	ΔT_x (°C)	T_{rg}	γ	Formation method	Reference
$Ni_{59}Ta_{41}$	2	720	783	63	–	–	SC	[64]
$Ni_{61}Ta_{39}$	2	720	770	50	–	–	SC	[64]
$Ni_{60}Ta_{40}$	–	720	777	57	–	–	MS	[65]
$Ni_{60}Nb_{40}$	–	–	–	–	–	–	MS	[65]
$Ni_{62}Ta_{38}$	–	720	877[a]	157	–	–	MS	[66]
$Ta_{42}Ni_{42}Co_{16}$	–	725	765	40	0.627	0.401	SC	[67]
$Ta_{42}Ni_{40}Co_{18}$	2	720	759	39	0.623	0.399	SC	[67]
$Ta_{42}Ni_{38}Co_{20}$	–	730	765	35	0.628	0.399	SC	[67]
$Ta_{42}Ni_{36}Co_{22}$	–	732	762	30	0.621	0.395	SC	[67]
$Ta_{46}Ni_{36}Co_{18}$	–	718	754	35	–	–	SC	[67]
$Ta_{50}Ni_{32}Co_{18}$	–	707	742	35	–	–	SC	[67]
$W_{30}Fe_{38}B_{25}C_7$	–	775	794	19	–	–	MS	[70]
$W_{30}Fe_{38}B_{22}C_{10}$	–	712	730	18	–	–	MS	[70]
$W_{30}Fe_{38}B_{19}C_{13}$	–	696	714	18	–	–	MS	[70]
$W_{30}Fe_{38}B_{17}C_{15}$	–	695	711	16	0.607	–	MS	[70]
$Co_{59}Ta_6B_{35}$	1.5	661	708	47	0.620	0.401	MS, SC	[71]
$Co_{58}Ta_7B_{35}$	2	672	723	51	0.630	0.406	MS, SC	[71]
$Co_{57}Ta_8B_{35}$	2	678	732	54	0.640	0.411	MS	[71]
$Co_{56}Ta_9B_{35}$	2	688	747	59	0.630	0.409	MS, SC	[71]
$Co_{55}Ta_{10}B_{35}$	1	702	770	68	0.630	0.414	MS, SC	[71]
$Co_{57}B_{35}Ta_8$	2	676	728	52	0.636	0.410	MS	[72]
$Co_{54.5}B_{37.5}Ta_8$	1	697	753	56	0.642	0.414	MS	[72]
$Ni_{51}W_{31.6}B_{17.4}$	0.1	656	723	67	0.521	0.367	SC	[42]
$Ni_{46}Cu_5W_{31.6}B_{17.4}$	–	698	790	92	0.546	0.386	SC	[42]

[a]These values are anonymously high, and it is not clear how they were determined.

As is commonly reported, compositions near a eutectic point exhibited the highest GFA. Compositions with the best GFA had the lowest liquidus temperatures and exhibited only one crystallization peak during differential scanning calorimetry (DSC) analysis. These HTMGs exhibited d_c values as high as 2.5 mm. Increasing B content was found to increase T_g, T_x, and ΔT_x. Zhang *et al.* [63] explained this behavior by noting that a higher ΔH was observed at T_g when alloys with a higher B content were examined. This indicated that the supercooled liquid had better thermal stability as the amount of B in the alloy was increased. Addition of Ni was also found to improve GFA.

Along with GFA, strength increased with increasing B content due to an increase in the negative heats of mixing which led to stronger bonds. During compression testing, shear bands were found to be at a 44° angle to the compressive axis, demonstrating that shear deformation of this alloy was mainly controlled by primary shear stress. It was posited that the HTMGs in this system were good candidate materials for coatings due to their high hardness and lack of ferromagnetism.

III. T_x BETWEEN 750 °C AND 799 °C

The thermal properties of glass forming alloys with T_x between 750 °C and 799 °C are presented in Table III. Mechanical properties of the same alloys are presented in Table IV. Note that all alloys in a system were sorted into the same temperature category based on the maximum T_x value observed in that system. For example, several of the alloys in the W-Fe-B-C system have a T_x below 750 °C, but the entire system is discussed in this section as the maximum T_x was between 750 °C and 799 °C. This organizational scheme was followed to unify the discussion of each given alloy system.

Wang *et al.* [64] reported on the formation of Ni_xTa_{1-x} (x = 59, 60, 61, and 62) HTMGs. These binary compositions were chosen as the Ni-Ta phase diagram exhibits a relatively deep eutectic at around 38 at. % Ta. These alloys were fabricated with diameters of 2 mm using copper-mold suction casting. Using this technique, samples containing <58 at. % Ni or >63 at. % Ni showed varying amounts of crystallinity. Only samples in the range 59–62 at. % Ni were found to be fully glassy. In a study primarily focused on nanocrystallization at temperatures below T_g, Wang *et al.* [65] examined $Ni_{60}Ta_{40}$ and $Ni_{60}Nb_{40}$ HTMGs. Ni-Nb was chosen in addition to Ni-Ta as Ni-Nb shows a similarly deep eutectic at around 40 at. % Nb. Due to the low liquid stability of these compositions, phase-separation-like nanocrystallization was observed in both $Ni_{60}Ta_{40}$ and $Ni_{60}Nb_{40}$ at temperatures below the calorimetric glass transition. Zhang *et al.* [66] also studied a $Ni_{62}Ta_{38}$ binary HTMG, though samples were produced with a thickness of only 40 μm using a single-roller melt-spinning method. A T_x of 877 °C was reported, although this is much higher than the value reported for the same composition by Wang *et al.* [64] (777 °C) and it is not stated what measurement technique was used to obtain this value.

Meng *et al.* [67] found that the GFA of $Ta_{42}Ni_{42-x}Co_{16+x}$ was very sensitive to Co content. The samples in this study

TABLE IV. Selected mechanical properties of metallic glasses with crystallization temperatures (T_x) between 750 °C and 799 °C. H_v = Vickers microhardness, E = modulus of elasticity, σ_y = yield strength, σ_f = fracture strength, and ε_p = plastic strain limit.

Composition	H_v (GPa)	E (GPa)	H_v/E	$H_v^2/2E$ (GPa)	σ_y (GPa)	σ_f (GPa)	ε_p (%)	Reference
$Ni_{59}Ta_{41}$	9.5	175	0.0543	0.258	–	–	–	[64]
$Ni_{61}Ta_{39}$	9.5	175	0.0543	0.258	–	–	–	[64]
$Ni_{60}Ta_{40}$	–	–	–	–	–	–	–	[65]
$Ni_{60}Nb_{40}$	–	–	–	–	–	–	–	[65]
$Ni_{62}Ta_{38}$	–	–	–	–	–	–	–	[66]
$Ta_{42}Ni_{42}Co_{16}$	–	–	–	–	–	–	–	[67]
$Ta_{42}Ni_{40}Co_{18}$	9.74	170	–	–	2.6	–	–	[67]
$Ta_{42}Ni_{38}Co_{20}$	–	–	–	–	–	–	–	[67]
$Ta_{42}Ni_{36}Co_{22}$	–	–	–	–	–	–	–	[67]
$Ta_{46}Ni_{36}Co_{18}$	–	–	–	–	–	–	–	[67]
$Ta_{50}Ni_{32}Co_{18}$	–	–	–	–	–	–	–	[67]
$W_{30}Fe_{38}B_{25}C_7$	11.95	–	–	–	–	–	–	[70]
$W_{30}Fe_{38}B_{22}C_{10}$	12.35	–	–	–	–	–	–	[70]
$W_{30}Fe_{38}B_{19}C_{13}$	12.9	–	–	–	–	–	–	[70]
$W_{30}Fe_{38}B_{17}C_{15}$	12.78	–	–	–	–	–	–	[70]
$Co_{59}Ta_6B_{35}$	15.2	–	–	–	5.41	5.72	1.5	[71]
$Co_{58}Ta_7B_{35}$	15.4	240.6	0.0644	0.493	5.42	5.80	1.1	[71]
$Co_{57}Ta_8B_{35}$	15.5	240.1	0.0646	0.500	5.515	5.875	0.9	[71]
$Co_{56}Ta_9B_{35}$	15.9	246.9	0.0644	0.512	5.59	5.97	0.6	[71]
$Co_{55}Ta_{10}B_{35}$	16.1	–	–	–	5.63	6.02	0.5	[71]
$Co_{57}B_{35}Ta_8$	–	242	–	–	5.52	5.87	0.9	[72]
$Co_{54.5}B_{37.5}Ta_8$	–	249	–	–	5.75	2.97	0.2	[72]
$Ni_{51}W_{31.6}B_{17.4}$	12.41	–	–	–	–	–	–	[42]
$Ni_{46}Cu_5W_{31.6}B_{17.4}$	11.9	–	–	–	–	–	–	[42]

were produced through both single-roller melt spinning and copper-mold suction casting. With increasing Co content, T_g increased from 725 °C to 732 °C, while T_x remained relatively constant over the compositional range. γ values increased with increasing Ta content from 0.395 to 0.401. T_{rg} did not vary in a consistent way, with values ranging from 0.621 to 0.628. The highest d_c (2 mm) was obtained with the $Ta_{42}Ni_{40}Co_{18}$ alloy, although this alloy did not have the largest ΔT_x, γ, or T_{rg}.

The mechanical properties of Ta-based MGs can be attributed to Ta as it has high elastic moduli, strength, and density. $Ta_{42}Ni_{40}Co_{18}$ samples had a Vickers hardness (H_v) of 9.74, an elastic modulus (E) of ~170 GPa, and a density of 12.98 g/cm^3 [67]. The quantity H_v/E is used as an indicator of wear resistance with typical MGs exhibiting values on the order of 0.03–0.06 [68,69]. $H_v^2/2E$ was used to quantify the resilience of coatings with typical values for MGs lying between 0.0 and 0.6 GPa. With H_v/E values of ~0.05 and $H_v^2/2E$ of ~0.28 GPa, these alloys are not expected to make especially wear resistant or resilient coating materials. This alloy system also exhibits low Poisson's ratio (ν) values and, therefore, displays brittle behavior.

Figure 4 shows several bulk metallic glass (BMG) compositions including Co- and Ir-based MGs which exhibit steep drop-offs in strength as temperature is increased near T_g. In particular, the IrNiTa alloy shows exceptional strength >4 GPa and maintains that strength up to high temperatures, similar to the temperatures at which strength decreases in typically high temperature resistant alloys such as Inconel 718.

Suo *et al.* [70] produced alloys in the system $W_{30}Fe_{38}B_{32-x}C_x$ (x = 5, 7, 10, 13, 15) using low purity industrial raw materials such as ferrotungsten, ferroboron, and cast iron. The study specifically focused on observing the effects of varying the ratio of C to B. HTMG samples were

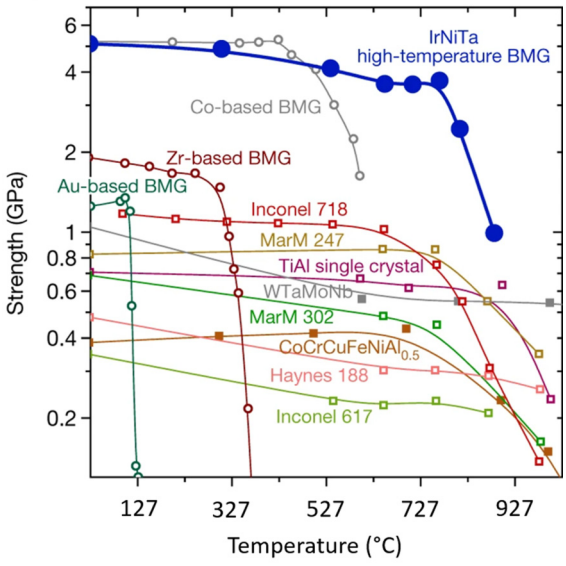

FIG. 4. Strength versus temperature of several high-temperature BMGs as well as a variety of alloy classes including high-temperature alloys; high-entropy alloys; and Au-, Zr-, and Co-based BMGs. Above 727 °C, the strength of IrNiTa high-temperature BMG drops off steeply. Reprinted from Ref. [75] with permission from Springer. Temperatures on the x axis have been converted from K to °C.

produced through single-roller melt spinning. At 10 at. % C, a fully glassy alloy was produced. Higher and lower amounts of W produced crystals when cooled through the same method. Due to limitations with the measurement techniques used in this study, T_l could not be determined for the majority of the alloys. T_{rg} was only calculated for $W_{30}Fe_{38}B_{17}C_{15}$ and had a value of 0.607. Crystallization temperature was gradually reduced with increasing C content, which also led to lower ΔT_x values. At 0.077 nm, C has a lower atomic radius than W (0.137 nm), Fe (0.124 nm), and B (0.09 nm). In addition, C has a negative heat of mixing with respect to the other three elements in the alloy. It was hypothesized that the strong cohesive forces between W-B, Fe-B, W-C, and Fe-C combined with the negative heats of mixing led to dense packing in the liquid state, which favored glass formation during solidification. The high crystallization temperature (711 °C–795 °C) and high hardness (11.9–12.9 GPa) in this alloy system were all attributed to the presence of W.

In a study by Wang *et al.* [71], increasing Ta content from 0 at. % to 7 at. % in the system $Co_{65-x}Ta_xB_{35}$ was shown to drastically improve d_c from 0.05 to 2.0 mm. Samples were created through both single-roller melt spinning and copper-mold injection casting. Generally, increases in Ta content increased T_g, T_x, ΔT_x, and both T_{rg} and γ. Alloys with 7–9 at. % Ta all had the same d_c value of 2 mm. The 10 at. % Ta samples had the highest γ value while exhibiting a d_c of only 1 mm. Yield and fracture strength of these alloys showed an increase up to 6 GPa with increasing Ta with a corresponding decrease in plastic strain limit from 1.5% to 0.5%. During compressive testing, the formation of many microcracks was observed before final failure, leading to a highly fragmented fracture. Wang *et al.* [71] discuss a possible correlation between plasticity and elastic properties. G/B (where G is the shear modulus and B is the bulk modulus) and ν (where ν is Poisson's ratio) were claimed to correlate with plastic deformation. HTMGs with G/B values below <0.43 or $\nu > 0.31$ are expected to exhibit significant plastic deformation. The values for the alloys in this study were $G/B = 0.42$ and $\nu = 0.315$, which falls within the ranges for the transition from plastic to brittle fracture behavior. After compressive testing, features of both brittle fracture and plastic fracture could be observed.

Wang *et al.* [72] also examined the same alloy system but now studied the effects of metalloid content on GFA and other properties. Alloys in the system $Co_{92-x}Ta_8B_x$ ($x = 30$, 32.5, 35, 37.5) were fabricated through single-roller melt spinning and copper-mold injection casting. Both T_g and T_x showed an increase with increasing B content. While the GFA parameters T_{rg} and γ exhibited a steady increase with increasing B content from 0.580 to 0.642 and from 0.380 to 0.414, respectively, they failed to predict the best glass former in the system. According to T_{rg} and γ, the best glass former should be at 37.5 at. % B. Experimentally, the greatest GFA was found in the 32.5 at. % B sample. The plastic strain limit was found to decrease with increasing B content, while yield and fracture strength slightly increased. The alloys in this system showed plastic strain limits as high as 2.5% and strengths up to 5.75 GPa. It was explained that decrease in shear modulus resulted in an increase in Poisson's ratio, leading to improved plasticity. Fracture surfaces after compressive testing showed that a small amount of ductile shear occurred before final brittle fracture. While samples with higher plasticity had decreased strength, the strengths greater than 5 GPa are still considered to be high. Simultaneous achievement of ultrahigh strength and good plasticity, as achieved in this system, is rare.

Hitit *et al.* [42] reported on $Ni_{51-x}Cu_xW_{31.6}B_{17.4}$ alloys which had a maximum $d_c < 400\ \mu$m. Using a piston and anvil method in an induction arc furnace, 100 and 400 μm samples were produced. The piston and anvil method is a technique in which thin foils were produced by squeezing a molten sample between two copper plates in an arc furnace. While 100 μm samples were fully x-ray amorphous, 400 μm samples showed significant crystallinity. The 400 μm samples contained Ni and W_2B crystalline phases. The observed Ni phase had a larger than normal lattice parameter, indicating that it was actually a Ni-W solid solution. In this study, and several others authored by Hitit, T_g values of several alloys were not reported. Hitit *et al.* stated that T_g of these alloys could not be well defined, and that reported T_g values were determined only tentatively. T_g and T_x were found to increase with addition of Cu. Cu is not soluble in W in the liquid state but is completely soluble in Ni. Ni and W are completely soluble in the liquid state. The authors posited that Cu substitution for Ni lowered the solubility of W in Ni in the liquid state, decreasing the number of Ni-W neighbors while increasing W-W and W-B neighbors. While increasing T_g and T_x with constant T_l is expected to increase GFA according to the parameters T_{rg} and γ, the GFA experimentally measured in this study did not follow that trend. This finding was a result of the ease with which the W_2B phase formed with the addition of Cu, leading more readily to crystallization.

IV. T_x OF 800 °C AND ABOVE

The thermal properties of glass forming alloys with T_x of 800 °C and above are presented in Table V. Mechanical properties of the same alloys are presented in Table VI. As in the previous section, all alloys in a given system were sorted into the same temperature category based on the maximum T_x value observed in that system.

Zhang *et al.* [73] developed a six-component $Mo_{44}Si_{26}Ta_5Zr_5Fe_3Co_{12}Y_5$ HTMG through mechanical alloying. Binary $Mo_{50}M_{50}$ alloys were initially created, where M = Ni, Fe, Co, and Si. After determining that amorphization occurred more readily in Mo-Co and Mo-Si, the ternary alloy Mo-Co-Si was selected for further study. In the series $Mo_y(Si_{0.7}Co_{0.3})_{100-y}$, the best glass formation was observed at y > 60. $Mo_6Si_{28}Co_{12}$ had the highest T_x value in the series but did not exhibit a distinct T_g. $Mo_6Si_{28}Co_{12}$ was selected as the base for alloying with other elements. Y was first selected due to its larger atomic radius. With an addition of 5 at. % Y, the diffraction peaks associated with Mo became less pronounced and a distinct T_g was observed. Further alloying with 10 at. % Ta and 5 at. % Zr increased the T_g, as well as the ΔT_x. No reason was provided for how these other elements were selected. Using XRD it was determined that the final $Mo_{44}Si_{26}Ta_5Zr_5Fe_3Co_{12}Y_5$ had an amorphous volume fraction of 100%, as estimated through fitting of XRD line profiles. With increasing number of components, GFA and the width of the supercooled liquid region were seen to

TABLE V. Selected thermal properties of metallic glasses with crystallization temperatures (T_x) of 800 °C and above. d_c = critical casting thickness, T_g = glass transition temperature, ΔT_x = supercooled liquid region, T_{rg} = reduced glass transition temperature (T_g/T_l), and $\gamma = T_x/(T_g + T_l)$. MS = melt spinning; SC = copper-mold suction casting.

Composition	d_c (mm)	T_g (°C)	T_x (°C)	ΔT_x (°C)	T_{rg}	γ	Formation method	Reference
$Mo_{55}Si_{28}Co_{12}Y_5$	–	863	971	108	–	–	MA	[73]
$Mo_{45}Si_{28}Ta_{20}Co_{12}Y_5$	–	865	990	125	–	–	MA	[73]
$Mo_{44}Si_{26}Ta_5Zr_5Fe_3Co_{12}Y_5$	–	929	1051	122	–	–	MA	[73]
$(Ni_{49.7}Cr_{14.7}B_{35.6})_{85}W_{15}$	<0.1	734	792	58	–	–	PA	[41]
$(Ni_{49.7}Cr_{14.7}B_{35.6})_{60}W_{40}$	<0.1	787	839	52	–	–	PA	[41]
$W_{25}Fe_{35}B_{30}$	<0.1	744	787	43	–	–	PA	[1]
$W_{27.5}Fe_{40}B_{32.5}$	<0.1	790	837	47	–	–	PA	[1]
$W_{27.5}Fe_{45}B_{27.5}$	<0.1	770	817	47	–	–	PA	[1]
$W_{30}Fe_{40}B_{30}$	<0.1	833	867	34	–	–	PA	[1]
$W_{30}Fe_{45}B_{25}$	<0.1	763	813	50	–	–	PA	[1]
$W_{32.5}Fe_{40}B_{27.5}$	<0.1	822	870	48	–	–	PA	[1]
$W_{35}Fe_{35}B_{30}$	<0.1	857	904	47	–	–	PA	[1]
$Re_{15}B_{35}Co_{50}$	1–2	662	717	55	–	–	MS	[74]
$Re_{20}B_{35}Co_{45}$	1–2	678	749	71	–	–	MS	[74]
$Re_{25}B_{35}Co_{40}$	1–2	697	763	66	–	–	MS	[74]
$Re_{30}B_{35}Co_{35}$	1–2	723	784	61	–	–	MS	[74]
$Re_{35}B_{35}Co_{30}$	1–2	748	805	57	–	–	MS	[74]
$Re_{40}B_{35}Co_{25}$	1–2	770	825	52	–	–	MS	[74]
$(Mo_{45}Ni_{45}Si_{10})_{90}B_{10}$	1.54	839	839	0	0.635	0.389	MS	[69]
$Ir_{25}Ni_{35}Ta_{40}$	–	812	892	80	0.581	0.404	SC	[75]
$Ir_{33}Ni_{28}Ta_{39}$	–	857	967	120	0.603	0.424	SC	[75]
$Ir_{35}Ni_{25}Ta_{40}$	2	889	992	103	0.630	0.431	SC	[75]
$Ir_{35}Ni_{20}Ta_{40}B_5$	3	874	1010	136	0.621	0.443	SC	[75]

TABLE VI. Selected mechanical properties of metallic glasses with crystallization temperatures (T_x) of 800 °C and above. H_v = Vickers microhardness, E = modulus of elasticity, σ_y = yield strength, σ_f = fracture strength, and ε_p = plastic strain limit.

Composition	H_v (GPa)	E (GPa)	H_v/E	$H_v^2/2E$ (GPa)	σ_y (GPa)	σ_f (GPa)	ε_p (%)	Reference
$Mo_{55}Si_{28}Co_{12}Y_5$	–	–	–	–	–	–	–	[73]
$Mo_{45}Si_{28}Ta_{20}Co_{12}Y_5$	–	–	–	–	–	–	–	[73]
$Mo_{44}Si_{26}Ta_5Zr_5Fe_3Co_{12}Y_5$	18	235	0.0765	0.689	6[a]	–	–	[73]
$(Ni_{49.7}Cr_{14.7}B_{35.6})_{85}W_{15}$	12.11	–	–	–	–	–	–	[41]
$(Ni_{49.7}Cr_{14.7}B_{35.6})_{60}W_{40}$	13.73	–	–	–	–	–	–	[41]
$W_{25}Fe_{35}B_{30}$	13.14	–	–	–	–	–	–	[1]
$W_{27.5}Fe_{40}B_{32.5}$	15.15	–	–	–	–	–	–	[1]
$W_{27.5}Fe_{45}B_{27.5}$	13.3	–	–	–	–	–	–	[1]
$W_{30}Fe_{40}B_{30}$	15.77	–	–	–	–	–	–	[1]
$W_{30}Fe_{45}B_{25}$	14.56	–	–	–	–	–	–	[1]
$W_{32.5}Fe_{40}B_{27.5}$	15.14	–	–	–	–	–	–	[1]
$W_{35}Fe_{35}B_{30}$	16.02	–	–	–	–	–	–	[1]
$Re_{15}B_{35}Co_{50}$	15.5	240.4	0.064	0.499	–	6.339[a]	–	[74]
$Re_{20}B_{35}Co_{45}$	16.08	251	0.064	0.515	–	6.101[a]	–	[74]
$Re_{25}B_{35}Co_{40}$	16.84	264.9	0.064	0.535	–	5.810[a]	–	[74]
$Re_{30}B_{35}Co_{35}$	17.59	278.5	0.063	0.555	–	5.550[a]	–	[74]
$Re_{35}B_{35}Co_{30}$	18.32	293.9	0.062	0.571	–	5.417[a]	–	[74]
$Re_{40}B_{35}Co_{25}$	19.1	304.9	0.063	0.598	–	5.271[a]	–	[74]
$(Mo_{45}Ni_{45}Si_{10})_{90}B_{10}$	27.5	364.3	0.075	1.04	–	–	–	[69]
$Ir_{25}Ni_{35}Ta_{40}$	–	–	–	–	–	–	–	[75]
$Ir_{33}Ni_{28}Ta_{39}$	–	–	–	–	–	–	–	[75]
$Ir_{35}Ni_{25}Ta_{40}$	–	–	–	–	–	5.1	–	[75]
$Ir_{35}Ni_{20}Ta_{40}B_5$	15	263	0.057	0.423	–	–	–	[75]

[a]These values are calculated based on empirical formulas and were not measured directly.

generally increase [73]. This behavior was observed in this study, as the use of a wider range of different atomic sizes increased packing density and subsequently increased the stability of the supercooled liquid.

The effect of refractory metal content, specifically tungsten, on the GFA and mechanical properties of a HTMG was experimentally investigated by Hitit *et al.* in 2013 [41]. The $(Ni_{49.7}Cr_{14.7}B_{35.6})_{100-x}W_x$ ($x = 15$–40) alloys were produced through the piston and anvil method in an induction arc furnace. It was noted that the GFA of NiCrBW is low due to the high liquidus temperature of the alloy, with $d_c < 50\,\mu$m. Values for T_{rg} and γ were not reported and cannot be calculated as T_l values were not provided. The authors state that alloying additions to lower liquidus temperature could improve GFA. While the addition of W was found to lower GFA, it also increased the values of both T_x and T_g, potentially increasing the range of temperatures at which the alloys could be useful. This increase in thermal stability was explained by an increasing number of W-W and W-B bonds, which have a high bonding strength. This change in bonding strength was posited to also contribute to increasing H_v from 12.11 GPa to 13.73 GPa.

In 2015, Öztürk and Hitit developed alloys in the W-Fe-B system with a range of compositional values [1]. The critical casting thickness of WFeB alloys was found to be $<100\,\mu$m. Due to its high cooling rate, the piston and anvil method was used to enhance the chances for forming a glass, although this technique is not expected to be useful in producing parts for industrial applications. With increasing W and B, more W-W, B-B, and W-B bonds were formed, increasing the cohesive energy of the alloy which in turn increases the stability of the glassy phase. While increasing W and decreasing B leads to higher T_x (up to 904 °C), the effect appeared to plateau at a certain W content as the increase in cohesive energy brought on by the increase in W-W bonds was balanced by the decrease in W-B and B-B bonds. The increase in W and B was also shown to increase the hardness of the alloys from 13.14 to 16.02 GPa in the samples with the most W and B. Increase in the number of strong bonds (e.g., W-W, W-B, and B-B) was also thought to be the origin of the observed hardness increase.

Wang *et al.* [74] fabricated and studied $Re_{65-x}B_{35}Co_x$ ($x = 25$, 30, 35, 40, 45, 50) HTMGs. Samples were produced through single-roller melt spinning at a uniform thickness of $\sim 20\,\mu$m. GFA was not experimentally determined and T_{rg} and γ values were not reported. ΔT_x values in this system ranged from 5 °C to 66 °C. While this is not directly indicative of high GFA, it shows good liquid stability and possible suitability for thermoplastic forming applications. Very high hardness, as high as 19.10 GPa, was observed. H_v was found to decrease with increasing Co content. High values of H_v were considered to relate to the strong bonding force among constituent elements of the alloy.

Kim *et al.* [69] examined the properties of Mo-Ni-Si-B HTMG alloys in 2016. Over the compositional range of $(Mo_{45}Ni_{45}Si_{10})_{100-x}B_x$ ($x = 0$, 2, 5, 7, 10), samples with less than 7 at. % B were found to be nanocrystalline when fabricated using a melt spinning process. The addition of B up to 7 at. % produced partially amorphous samples. Samples with 10 at. % B were fully glassy. The nanocrystalline samples were found to follow a Hall-Petch type relation in which reduction

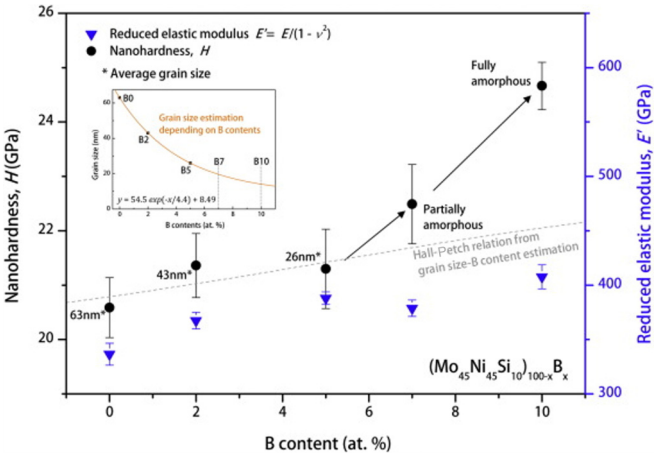

FIG. 5. Nanohardnesses and reduced elastic moduli of as-spun $(Mo_{45}Ni_{45}Si_{10})_{100-x}B_x$ samples depending on boron contents. (Inset) Grain size variation of as-spun $(Mo_{45}Ni_{45}Si_{10})_{100-x}B_x$ samples depending on boron contents, with an orange exponential fitting line. Nanocrystalline samples generally follow the Hall-Petch relation, where hardness increases with decreasing grain size. Partially glassy and fully glassy samples deviated from the Hall-Petch relation, with increasingly glassy samples showing increasingly high hardness. Reprinted from Ref. [69] with permission from Elsevier.

in grain size correlated with increased H_v as shown in Fig. 5. With increasing B content, samples became partially and then fully glassy. Upon loss of crystallinity, the hardness values increasingly deviated to higher hardness values from the relation observed in the nanocrystalline samples. The hardness values reported by Kim *et al.* are the highest among HTMGs that have been reported in the last 10 years, with a value of 27.5 GPa. B was chosen for this alloy due to its large negative heat of mixing relative to Mo, Ni, and Si, as well as its difference in atomic size [69]. This phenomenon was described in terms of large normalized mismatch entropy (S_σ/k_B, where S_σ is the mismatch entropy and k_B is the Boltzmann constant); a large atomic size distribution range leads to a higher degree of normalized mismatch entropy, subsequently stabilizing the glassy phase against corresponding crystalline phases. The HTMGs in this system have high hardness similar to ceramics, but with a much lower Young's modulus. High hardness with low elastic modulus is often indicative of a good coating material, as this can lead to a smaller elasticity mismatch with typical substrates. The MoNiSiB HTMGs showed an H_v/E value of 0.075 and an $H_v^2/2E$ value of 1.04 GPa. In MGs, both of these parameters show a general increase with increasing T_x value as shown in Fig. 6.

Li *et al.* [75] developed Ir-Ni-Ta-(B) alloys through a combinatorial method. This system was chosen, in part, due to the fact that all four elements have negative heats of mixing with respect to each other. Magnetron sputtering was initially used to form alloys in the desired compositional range. Once it had been determined through DSC that the critical cooling rates in this system were relatively low, larger samples were produced through coper-mold suction casting, and produced samples with diameters as large as 3 mm. $Ir_{35}Ni_{25}Ta_{40}$ exhibited one of the highest T_g values for any HTMG at 889 °C. Alloys with a small amount of B had supercooled liquid regions as large

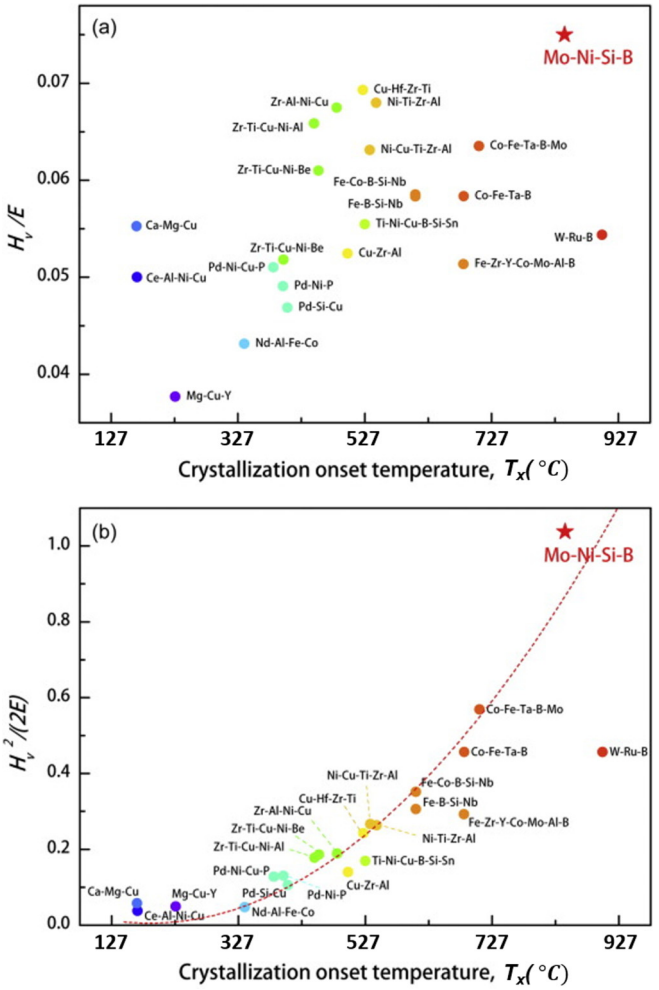

FIG. 6. (a) H/E and (b) $H_2/(2E)$ values of various glass forming alloy systems depending on T_x. HTMGs such as Mo-Ni-Si-B show better wear resistance and resilience, improving performance as a coating material. Reprinted from Ref. [69] with permission from Elsevier. Temperatures on the x axis have been converted from K to °C.

as 136 °C in the $Ir_{35}Ni_{20}Ta_{40}B_5$ samples, making them suitable for applications involving thermoplastic forming, while still having T_g (874 °C) and T_x (1010 °C) values suitable for use in high temperature applications. Thermoplastic forming was demonstrated by heating 1 mm diameter rods to the supercooled liquid region and rapidly drawing them out to form ∼45 μm wires. The samples of $Ir_{35}Ni_{20}Ta_{40}B_5$ had a hardness of 15 GPa and an elastic modulus of 263 GPa. The strength of $Ir_{35}Ni_{20}Ta_{40}B_5$ at 727 °C was 3.7 GPa, higher than that of most normal and high entropy alloys at similar temperatures. Other mechanical properties were tested at room temperature. A few corrosion weight-loss experiments were also performed, comparing the Ir-Ni-Ta-B alloys to stainless steel 304, as well as Zr- and Fe-based MGs. During oxidation tests in air, no substantial weight change was observed up to 797 °C, very near T_g. When submerged in aqua regia, fully glassy $Ir_{35}Ni_{25}Ta_{40}$ HTMG showed no weight loss after 112 days of immersion, while the partially crystalline version of the same alloys exhibited weight loss after 28 days; in comparison, Zr- and Fe-based MGs, as well as stainless steel 304, had experienced significant corrosion within an hour.

V. OUTLOOK AND FUTURE WORK

In reviewing the above literature, one can see that there exist several knowledge gaps with respect to HTMGs. This section discusses properties that have not been widely characterized and studied, as well as an outlook for future developments for improving high-temperature stability of MGs.

A. GFA decreases with increasing T_x

Examining the above literature, one will note that the HTMGs reported in the "T_x of 800 °C and above" category have small d_c values, often less than 1 mm. As previously mentioned, high T_x correlates with high melting temperature of an alloy's constituent elements, but high T_l also leads to lower GFA according to both T_{rg} and γ. As GFA is reduced, the rate at which an alloy must be cooled to achieve a glassy state is increased. This phenomenon leads to a lower critical casting thickness, as samples with larger dimensions cannot be cooled quickly and uniformly, and is the major issue facing HTMGs, as well as MGs in general [70,76,77]. Increasing the GFA of HTMGs has been approached in many ways in the literature reported in this article. These include atomic size mismatch, high negative heats of mixing between alloy components, the use of many components in an alloy, and design of glass composition such that complex crystalline phases are thermodynamically favored.

In general, the GFA of a glassy system is improved when the thermodynamic driving force for crystallization is low. Making use of this principle, MGs are often designed such that the energetically favored crystalline phase is complex and long-range atomic rearrangement is required for it to form from the liquid phase. This behavior was demonstrated in the study by Zhang *et al.* [73] in which elements were added to an MG in a stepwise fashion. As the number of components in the alloy increased, samples became increasingly x-ray amorphous. The additional elements were also of varying atomic sizes, further increasing the free energy of potential crystalline phases and increasing GFA. Zhang *et al.* [63] reported that the formation of complex or competing crystalline phases was also an effective way of increasing the stability of the supercooled liquid phase and thus improving GFA.

Similarly, the thermodynamic driving force for crystallization can be lowered by increasingly negative heats of mixing between alloy components. As ΔH_m becomes more negative, crystallization is less thermodynamically favored and thus glass formation can occur at lower cooling rates. Several of the studies reported in this article mentioned a high negative ΔH_m as a major factor in increasing GFA [53,69,70].

Another method by which GFA is often increased is by lowering the free energy of the supercooled liquid phase, and thus lowering the thermodynamic driving force for crystallization. Lowering of free energy is often accomplished in MGs by using atomic species with a wide range of atomic radii. Significant differences in atomic size between constituents of an alloy results in efficient packing of clusters and increased

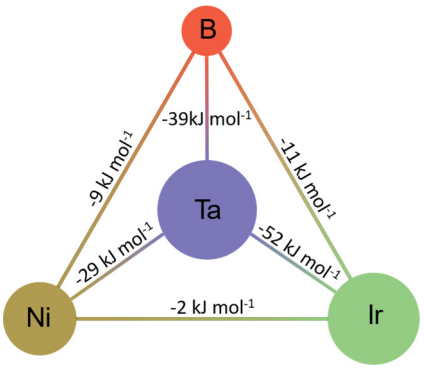

FIG. 7. The heat of mixing between the elements used by Li *et al.* [65] is shown. Relative size difference of the atoms is indicated by the size of the circles.

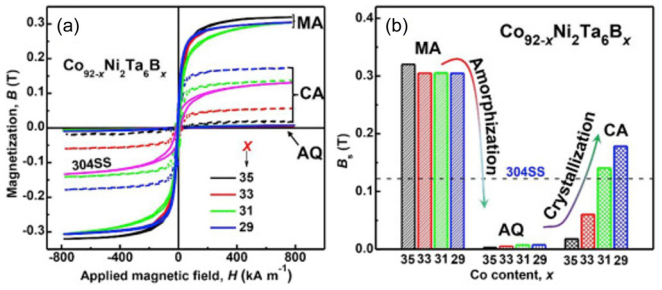

FIG. 8. Hysteresis *B*-*H* loops of $Co_{92-x}Ni_2Ta_6B_x$ ($x = 35, 33, 31, 29$) master alloys (MA), as-quenched (AQ), and crystallized alloy (CA) ribbons. Crystalline MA samples show strong magnetization. As-quenched glassy samples have greatly reduced magnetization. CA samples recover strong magnetic feature to varying degrees. While Co content does not appear to have an effect on MA samples, CA samples show increasing magnetization with decreasing Co content. Reproduced from Ref. [63] with permission from Elsevier.

density of random packing of atoms in the supercooled liquid state [17]. Wang *et al.* made specific mention of this phenomenon when discussing their Co-Ir-Ta-B HTMGs, in which the variety of atomic sizes is said to lead to a higher degree of short-range order in the supercooled liquid phase [51]. Kim *et al.* discussed the same phenomenon in terms of normalized mismatch entropy, as discussed previously [69]. Figure 7 demonstrates how the use of both negative heats of mixing and atomic radius mismatch were used in selecting components for the Ir-Ni-Ta-(B) alloy studied by Li *et al.* [75]. Making use of the method of lowering the free energy of the supercooled liquid has allowed for the development of HTMGs with higher T_x values.

Frequently, the structural effects of such methods of increasing GFA are observed through XRD of the crystalline phases that form at cooling rates or compositions where GFA is low. Notably missing from the existing literature on HTMGs are studies which directly examine the structure of the glassy phase itself. It is recommended that techniques such as neutron diffraction or extended x-ray absorption fine structure (EXAFS) be utilized to study the structure of the glassy phase. These techniques also often lend themselves to *in situ* studies while the material is heated/cooled which can provide information on structural rearrangement. Likely these techniques are used less frequently due to their relatively scarce access and higher difficulty in data analysis when compared to more common laboratory-based techniques. However, such analyses would allow researchers to observe changes in short- and intermediate-range order caused by the addition of alloying elements and may lead to a greater understanding of the mechanisms for improving GFA.

We predict that the above recommended characterization studies, in conjunction with thermodynamic phase modeling and machine learning techniques, can be used to predict and synthesize glass forming alloys with better high temperature properties.

B. Magnetic properties

While the cost of producing bulk HTMG parts for structural applications may be high, one potential cost-saving application is use as coating materials. As discussed in this article, HTMGs are attractive coating materials due to their high hardness, wear resistance, and resilience. However, Fe-based HTMG systems are potentially ferromagnetic. In coating materials, this ferromagnetism is undesirable as it may cause disturbances with other ferromagnetic parts [63].

The study of $Co_{92-x}Ni_2Ta_6B_x$ alloys by Zhang *et al.* [63] reported on this system's magnetic properties. "Master alloys" (MAs), which were crystalline alloys in the system, showed strong magnetic hysteresis. Upon quenching to form a glass, as-quenched (AQ) samples showed a nearly complete loss of ferromagnetism. Upon heat treatment to achieve recrystallization, crystallized alloy (CA) samples with low B content samples recovered the strong magnetic feature. When B content was high, CA samples did not recover the strong magnetism to the same extent. This behavior is shown in Fig. 8(b). Co content was not found to affect magnetization of MA or AQ samples to a large extent, but strongly affected CA samples. Thus, HTMGs in this system are good candidate materials for coatings due to their high hardness and lack of ferromagnetism. When compared to CA in the same systems and to stainless steel 304, the magnetization of the HTMGs is much lower.

Also relevant for materials intended for high temperature applications are changes in magnetization with increasing temperature. One potential application of such magnetocaloric materials, as discussed by Zhang *et al.* [53], is in environmentally friendly and energy efficient refrigeration. In their $Fe_{68-x}Cr_xNb_4Y_6B_{22}$ ($x = 2$–6) system, increasing Cr content was found to shift the magnetic transition temperature to lower values. This is likely due to an antiferromagnetic interaction between Fe and Cr atoms. Increasing Cr content was also observed to lower the saturation magnetization.

We were unable to find other studies measuring the magnetic and magnetocaloric properties of HTMGs. Thus, a significant research opportunity exists in studying the magnetization of a wider range of HTMGs at high temperatures in order to ascertain the usefulness of such materials in applications in which a lack of magnetic disturbances may be critical to operation, such as in housings for sensors designed for use in extreme environments.

C. Measuring mechanical properties at high temperatures

In all but one study presented in this article, mechanical properties of the HTMG samples were measured at or near room temperature. As one of the major applications of HTMGs is in high-temperature environments, the room temperature mechanical properties are not direct indicators of performance in the intended service environment.

The single study which measured mechanical properties of an HTMG at high temperature was by Li *et al.* in 2019 [75]. As noted above, they showed that their alloy maintained a high strength at an elevated temperature ($\geqslant$800 °C) at which most MGs would not be functional. Other properties such as plasticity, hardness, toughness, and elastic modulus were measured at room temperature, making a true evaluation of this alloy for high-temperature use difficult. Several studies of other MGs and high entropy alloys have reported on mechanical properties at high temperatures, though these have mainly focused on measuring creep resistance in MGs with lower T_x than those of interest in this review [78–80].

Two main factors appear to have prevented measurement of these high temperature properties in past studies. First is the lack of materials testing apparatus equipped with furnaces capable of reaching the necessary temperatures at research facilities. Second, many of the studies discussed in this article, despite examining materials with high T_x and high strengths, were focused only on low temperature structural applications or high temperature nonstructural applications and therefore do not make a point of characterizing mechanical properties at high-temperatures. Studies comparing high temperature mechanical properties of HTMGs to crystalline alloys of the same composition would be of great interest and could drive further research by demonstrating the potential of these materials. While these studies will likely require custom designed equipment, they will not be expensive as more research on molten salts, supercritical water, and high-temperature oxidation are being performed at academic institutions now.

As stated before, the high-temperature stability of MGs is one of the critical issues facing their wide industrial application. As more HTMGs are developed with higher T_x values, it is important that mechanical properties are measured in the temperature range in which the alloys will be utilized.

D. Corrosion resistance of high temperature metallic glasses

Corrosion resistance is often touted as an advantage of MGs over traditional crystalline alloys. Of the literature reported in this article, only the study by Li *et al.* on Ir-Ni-Ta-(B) glasses reported on corrosion [75]. The Ir-Ni-Ta-(B) MGs showed excellent corrosion resistance at high temperatures and also in challenging environments, such as aqua regia. Corrosion properties are of particular interest when discussing MGs for high-temperature applications as corrosion rate generally increases with temperature [81]. In some applications, the usefulness of an alloy is not limited by its thermodynamic and mechanical properties, but by its resistance to corrosion at high temperatures well below the melting point [7,8].

Most crystalline alloys experience significant corrosion at temperatures well below their melting point and thus have a limited temperature range in which they can be utilized. For example, stainless steels 304 and 316L have high melting points in the range of 1375 °C–1450 °C [82] but their implementation is limited by the fact that they often corrode at temperatures below 700 °C in strongly oxidative or reductive environments [8,83]. However, HTMGs are promising materials in such scenarios as many have been shown to maintain their strengths up to temperatures near T_g and are expected to experience less corrosion than crystalline alloys [75].

While the corrosion behavior of HTMGs has not been widely studied, several studies have shown that traditional MGs have improved corrosion resistance over crystalline alloys to varying degrees depending on the specific alloy system and environment [23,24,75]. For example, Gostin *et al.* [25] compared the corrosion resistance of a bulk glassy Fe-based alloy to that of a crystalline alloy of the same composition and a conventional steel alloy. The glassy alloy showed better pitting resistance and general stability than both crystalline alloys in chloride-containing electrolytes. While the fully glassy alloy had superior corrosion resistance to the crystalline alloy of the same composition in all environments studied, highly reactive elements (e.g., Mo, Mn, and Co) present in both caused the corrosion resistance to be superior to that of conventional steel in environments where passivation was achieved and inferior in others. Wang *et al.* [26] found that single-crystal Zr_2Ni samples had a lower corrosion resistance than a bulk metallic glass of the same composition. Electrochemical measurements performed in this study revealed that passive films formed on the amorphous alloy were more compact and less defective than those that formed on the single crystal. As previously mentioned, Li *et al.* [75] showed that bulk glassy Ir-Ni-Ta-(B) alloys had superior corrosion resistance compared to a recrystallized version of the same alloy. Several mechanisms contributing to the improved corrosion resistance of HTMGs have been hypothesized, though one commonly discussed reason is that the lack of crystallinity removes common sites for the initiation of localized corrosion such as grain boundaries and crystalline defects [84]. Intergranular corrosion is especially common at high temperatures, as diffusion can occur and allow for the precipitation of less corrosion resistant phases along the grain boundaries [85]. As MGs lack grain boundaries, they are not susceptible to this type of corrosion. High-temperature corrosion resistance of MGs is promising for many applications but has not yet been widely studied. HTMGs might especially be suitable for applications in challenging high-temperature environments for which no traditional crystalline alloy is available.

ACKNOWLEDGMENTS

The authors acknowledge the University of Utah's Research Incentive Seed Grant Program and the Roger and Dawn Crus Center for Metallurgy Student Research for financial support.

[1] P. Öztürk and A. Hitit, Effects of tungsten and boron contents on crystallization temperature and microhardness of tungsten based metallic glasses, Acta Metall. Sin. (Engl. Lett.) **28**, 733 (2015).

[2] D. V. Louzguine-Luzgin, M. Ito, S. V. Ketov, A. S. Trifonov, J. Jiang, C. L. Chen, and K. Nakajima, Exceptionally high nanoscale wear resistance of a $Cu_{47}Zr_{45}Al_8$ metallic glass with native and artificially grown oxide, Intermetallics **93**, 312 (2018).

[3] J. Bhatt, S. Kumar, C. Dong, and B. S. Murty, Tribological behaviour of $Cu_{60}Zr_{30}Ti_{10}$ bulk metallic glass, Mater. Sci. Eng.: A **458**, 290 (2007).

[4] H. Ludewig, J. R. Powell, M. Todosow, G. Maise, R. Barletta, and D. G. Schweitzer, Design of particle bed reactors for the space nuclear thermal propulsion program, Prog. Nucl. Energy **30**, 1 (1996).

[5] D. C. Hofmann, Bulk metallic glasses and their composites: A brief history of diverging fields, J. Mater. **2013**, 517904 (2013).

[6] J. E. Indacochea, J. L. Smith, K. R. Litko, and E. J. Karell, Corrosion performance of ferrous and refractory metals in molten salts under reducing conditions, J. Mater. Res. **14**, 1990 (1999).

[7] L. K. H. Leung, M. Yetisier, and W. Diamond, A next generation heavy water nuclear reactor with supercritical water as coolant, in *Proceedings of International Conference on Future of Heavy Water Reactors (HWR-FUTURE)* (Canadian Nuclear Society, Toronto, 2011), p. 815.

[8] S. Guo, J. Zhang, W. Wu, and W. Zhou, Corrosion in the molten fluoride and chloride salts and materials development for nuclear applications, Prog. Mater Sci. **97**, 448 (2018).

[9] D. Rodriguez, A. Merwin, and D. Chidambaram, On the oxidation of stainless steel alloy 304 in subcritical and supercritical water, J. Nucl. Mater. **452**, 440 (2014).

[10] A. Merwin and D. Chidambaram, The effect of Li^0 on the corrosion of stainless steel alloy 316L exposed to molten LiCl-Li_2O-Li, Corros. Sci. **126**, 1 (2017).

[11] W. Phillips and D. Chidambaram, Corrosion of stainless steel 316L in molten LiCl-Li_2O-Li, J. Nucl. Mater. **517**, 241 (2019)

[12] D. Rodriguez, A. Merwin, Z. Karmiol, and D. Chidambaram, Surface chemistry and corrosion behavior of Inconel 625 and 718 in subcritical, supercritical, and ultrasupercritical water, Appl. Surf. Sci. **404**, 443 (2017).

[13] T. Ghidini, Materials for space exploration and settlement, Nat. Mater. **17**, 846 (2018).

[14] A. Iveković, N. Omidvari, B. Vrancken, K. Lietaert, L. Thijs, K. Vanmeensel, J. Vleugels, and J. Kruth, Selective laser melting of tungsten and tungsten alloys, Int. J. Refract. Met. Hard Mater. **72**, 27 (2018).

[15] C. Ren, Z. Fang, M. Koopman, B. Butler, J. Paramore, and S. Middlemas, Methods for improving ductility of tungsten—a review, Int. J. Refract. Met. Hard Mater. **75**, 170 (2018).

[16] M. Zhao, W. Pan, C. Wan, Z. Qu, Z. Li, and J. Yang, Defect engineering in development of low thermal conductivity materials: A review, J. Eur. Ceram. Soc. **37**, 1 (2017).

[17] J.-Y. Kim, D. Jang, and J. R. Greer, Nanolaminates utilizing size-dependent homogeneous plasticity of metallic glasses, Adv. Funct. Mater. **21**, 4550 (2011).

[18] T. Gloriant, Microhardness and abrasive wear resistance of metallic glasses and nanostructured composite materials, J. Non-Cryst. Solids **316**, 96 (2003).

[19] C. Suryanarayana and A. Inoue, *Bulk Metallic Glasses* (CRC Press, Boca Raton, FL, 2017).

[20] A. L. Greer, Metallic glasses, in *Physical Metallurgy*, 5th ed., edited by D. E. Laughlin and K. Hono (Elsevier, Oxford, 2014), Chap. 4, p. 305.

[21] A. K. Varshneya and J. C. Mauro, Introduction, in *Fundamentals of Inorganic Glasses*, 3rd ed., edited by A. K. Varshneya and J. C. Mauro (Elsevier, Amsterdam, Netherlands, 2019), Chap. 1, p. 1.

[22] C. Schuh, T. C. Hufnagel, and U. Ramamurty, Mechanical behavior of amorphous alloys, Acta Mater. **55**, 4067 (2007).

[23] M. D. Demetriou, M. E. Launey, G. Garret, J. P. Schramm, D. C. Hofmann, W. L. Johnson, and R. O. Ritchie, A damage-tolerant glass, Nat. Mater. **10**, 123 (2011).

[24] M. Wakeda, J. Saide, J. Li, and S. Ogata, Controlled rejuvenation of amorphous metals with thermal processing, Sci. Rep. **5**, 10545 (2015).

[25] P. F. Gostin, A. Gebert, and L. Schultz, Comparison of the corrosion of bulk amorphous steel with conventional steel, Corros. Sci. **52**, 273 (2010).

[26] D. P. Wang, S. L Wang, and J. Q. Wang, Relationship between amorphous structure and corrosion behaviour in a Zr–Ni metallic glass, Corros. Sci. **59**, 88 (2012).

[27] W. J. Botta, J. E. Berger, C. S. Kiminami, V. Roche, R. P. Nogueira, and C. Bolfarini, Corrosion resistance of Fe-based amorphous alloys, J. Non-Cryst. Solids **586**, S105 (2014).

[28] C. A. C. Souza, D. V. Ribeiro, and C. S. Kiminami, Corrosion resistance of Fe-Cr-based amorphous alloys: An overview, J. Non-Cryst. Solids **442**, 56 (2016).

[29] M. Tavoosi and A. Barahimi, Corrosion behavior of amorphous–nanocrystalline Fe–Ni–Cr electrodeposited coatings, Surf. Interfaces **8**, 103 (2017).

[30] A. Gebert, Corrosion behaviour of magnesium (Mg)-based bulk metallic glasses, in *Corrosion of Magnesium Alloys*, edited by G.-L. Song (Woodhead Publishing, Cambridge, 2011), Chap. 5, p. 207.

[31] C. Örnek, C. Legraf, and J. Pan, Passive film characterisation of duplex stainless steel using scanning Kelvin probe force microscopy in combination with electrochemical measurements, npj Mater. Degrad. **3**, 8 (2019).

[32] J. Fornell, N. V. Steenberge, A. Varea, R. Rossinyol, E. Pellicer, S. Suriñach, M. D. Baró, and J. Sort, Enhanced mechanical properties and *in vitro* corrosion behavior of amorphous and devitrified $Ti_{40}Zr_{10}Cu_{38}Pd_{12}$ metallic glass, J. Mech. Behav. Biomed. Mater. **4**, 1709 (2011).

[33] X. Liu, Z. Xiang, J. Niu, K. Xia, Y. Yang, B. Yan, and W. Lu, The corrosion behaviors of amorphous, nanocrystalline and crystalline Ni-W alloys coating, Int. J. Electrochem. Sci. **10**, 9042 (2015).

[34] J. R. Scully and A. Lucente, Corrosion of amorphous metals, in *ASM Handbook Volume 13B* (ASM International, Materials Park, Ohio, 2005), p. 476.

[35] M. Yamasaki, S. Kagao, and Y. Kawamura, Thermal diffusivity and conductivity of supercooled liquid in $Zr_{41}Ti_{14}Cu_{12}Ni_{10}Be_{23}$ metallic glass, Appl. Phys. Lett. **84**, 4653 (2004).

[36] J. Kim, Weldability of $Cu_{54}Zr_{22}Ti_{18}Ni_6$ bulk metallic glass by ultrasonic welding processing, Mater. Lett. **130**, 160 (2014).

[37] Y. Shen, Y. Li, C. Chen, and H.-L. Tsai, 3D printing of large, complex metallic glass structures, Mater. Des. **117**, 213 (2017).

[38] Y. Lv and Q. Chen, Internal friction behavior and thermal conductivity of Fe-based bulk metallic glasses with different crystallization, Thermochim. Acta **666**, 36 (2018).

[39] A. L. Moore and L. Shi, Emerging challenges and materials for thermal management of electronics, Mater. Today **17**, 163 (2014).

[40] M. Bakkal, A. H. Shih, S. B. McSpadden, C. T. Liu, and R. O. Scattergood, Light emission, chip morphology, and burr formation in drilling the bulk metallic glass, Int. J. Mach. Tool. Manuf. **45**, 741 (2005).

[41] A. Hitit, P. Öztürk, H. Şahin, and A. M. Aşgın, Effect of tungsten content on glass forming ability and microhardness of Ni-Cr-B-W metallic glasses, J. Achiev. Mater. Manuf. Eng. **62**, 5 (2013).

[42] A. Hitit, H. Şahin, P. Öztürk, and A. M. Aşgın, A new Ni-based metallic glass with high thermal stability and hardness, Metals **5**, 162 (2015).

[43] K. J. Laws, B. Gun, and M. Ferry, Influence of casting parameters on the critical casting size of bulk metallic glass, Metall. Mater. Trans. A **40**, 2377 (2009).

[44] S. M. Song, Y. C. Liao, T. H. Li, C. K. Lee, P. H. Tsai, J. S. C. Jang, and J. C. Huang, Thermoplastic deformation behavior of a Fe-based bulk metallic glass within the supercooled liquid region, J. Mater. Res. Technol. **8**, 1907 (2019).

[45] X. H. Du, J. Huang, C. T. Liu, and Z. P. Lu, New criterion of glass forming ability for bulk metallic glasses, J. Appl. Phys. **101**, 086108 (2007).

[46] S. Guo, Z. P Lu, and C. T. Liu, Identify the best glass forming ability criterion, Intermetallics **18**, 883 (2010).

[47] Z. P. Lu, Y. Li, and S. C. Ng, Reduced glass transition temperature and glass forming ability of bulk glass forming alloys, J. Non-Cryst. Solids **270**, 103 (2000).

[48] M. Hasanuzzaman, A. Rafferty, M. Sajjia, and A. Olabi, Properties of glass materials, in *Materials Science and Materials Engineering* (Elsevier, Amsterdam, 2016), Reference module.

[49] A. K. Varshneya and J. C. Mauro, *Fundamentals of Inorganic Glasses* (Elsevier, Amsterdam, 2019).

[50] A. I. Popov, What is glass? J. Non-Cryst. Solids **502**, 249 (2018).

[51] J. Wang, L. Huang, S. Zhu, Q. Li, S. Guan, and T. Zhang, Glass-forming ability, fragility parameter, and mechanical properties of Co–Ir–Ta–B amorphous alloys, J. Alloys Compd. **576**, 375 (2013).

[52] L. Zhang, Y.-Q. Cheng, A.-J. Cao, J. Xu, and E. Ma, Bulk metallic glasses with large plasticity: Composition design from the structural perspective, Acta Mater. **57**, 1154 (2009).

[53] M. Zhang, J. Li, F. Kong, and J. Liu, Magnetic properties and magnetocaloric effect of FeCrNbYB metallic glasses with high glass-forming ability, Intermetallics **59**, 18 (2015).

[54] L. Yang, X. Meng, and G. Guo, Structural origin of the pinpoint-composition effect on the glass-forming ability in the NiNb alloy system, J. Mater. Res. **28**, 3170 (2013).

[55] K. Vijay Reddy and S. Pal, Contribution of Nb towards enhancement of glass forming ability and plasticity of Ni-Nb binary metallic glass, J. Non-Cryst. Solids **471**, 243 (2017).

[56] M. K. He, S. H. Chen, P. Yu, and L. Xia, Enhanced mechanical properties of $Ni_{62}Nb_{38}$ bulk metallic glasses by Ta substitution, J. Non-Cryst. Solids **471**, 452 (2017).

[57] L. Xia, S. T. Shan, D. Ding, and Y. D. Dong, Binary bulk metallic glass $Ni_{62}Nb_{38}$ with high compressive strength of 3100 MPa, Intermetallics **15**, 1046 (2007).

[58] H. Kimura, A. Inoue, X. Yamaura, K. Sasamori, M. Nishida, Y. Shinpo, and H. Okouchi, Thermal stability and mechanical properties of glassy and amorphous Ni-Nb-Zr alloys produced by rapid solidification, Mater. Trans. **44**, 1167 (2003).

[59] A. Inoue, W. Zhang, and T. Zhang, Thermal stability and mechanical strength of bulk glassy Ni-Nb-Ti-Zr alloys, Mater. Trans. **43**, 1952 (2002).

[60] S. Pang, T. Zhang, K. Asami, and A. Inoue, Bulk glassy Ni(Co–)Nb–Ti–Zr alloys with high corrosion resistance and high strength, Mater. Sci. Eng.: A **375-377**, 368 (2004).

[61] W. Zhang and A. Inoue, Formation and mechanical properties of Ni-based Ni–Nb–Ti–Hf bulk glassy alloys, Scr. Mater. **48**, 641 (2003).

[62] L. Y. Chen, H. Hu, Z. Guangzue, and J. Jiang, Catching the Ni-based ternary metallic glasses with critical diameter up to 3 mm in Ni–Nb–Zr system, J. Alloys Compd. **443**, 109 (2007).

[63] G. Zhang, H. Zhang, S. Yue, R. Cheng, A. Wang, A. He, Y. Dong, H. Ni, and C.-T. Liu, Preparation of non-magnetic and ductile Co-based bulk metallic glasses with high GFA and hardness, Intermetallics **107**, 47 (2019).

[64] Y. Wang, Q. Wang, J. Zhao, and C. Dong, Ni–Ta binary bulk metallic glasses, Scr Mater. **63**, 178 (2010).

[65] Y. Wang, Y. Li, J. Qiang, Y. Geng, Q. Wang, C. Dong, and S.-B. Mi, Nanocrystallization in $Ni_{60}Ta_{40}$ and $Ni_{60}Nb_{40}$ metallic glasses below calorimetric glass transition, J. Mater. Sci. **49**, 6007 (2014).

[66] X. Zhang, X. Mei, Y. Wang, Y. Wang, and J. Sun, The study of irradiation damage induced by proton in metallic glass $Ni_{62}Ta_{38}$ and metal W, Nucl. Instrum. Methods Phys. Res. Sect. B, **436**, 1 (2018).

[67] D. Meng, D. Q. Zhao, D. W. Ding, H. Y. Bai, M. X. Pan, and W. H. Wang, Tantalum based bulk metallic glasses, J. Non-Cryst. Solids **357**, 1787 (2011).

[68] A. Leyland and A. Matthews, On the significance of the *H*/*E* ratio in wear control: A nanocomposite coating approach to optimised tribological behaviour, Wear **246**, 1 (2000).

[69] J. Kim, J. S. Kyeong, M.-H. Ham, A. M. Minor, D. H. Kim, and E. Soo, Development of Mo-Ni-Si-B metallic glass with high thermal stability and *H* versus *E* ratios, Mater. Des. **98**, 31 (2016).

[70] Z. Y. Suo, Y. L. Song, B. Yu, and K. Q. Qiu, Fabrication of tungsten-based metallic glasses by low purity industrial raw materials, Mater. Sci. Eng.: A **528**, 2912 (2011).

[71] J. Wang, R. Li, N. Hua, and T. Zhang, Co-based ternary bulk metallic glasses with ultrahigh strength and plasticity, J. Mater. Res. **26**, 2072 (2011).

[72] J. Wang, L. Wang, S. Guan, S. Zhu, R. Li, and T. Zhang, Effects of boron content on the glass-forming ability and mechanical properties of Co–B–Ta glassy alloys, J. Alloys Compd. **617**, 7 (2014).

[73] X. Q. Zhang, E. Ma, and J. Xu, Mechanically alloyed multi-component Mo-based amorphous alloys with wide supercooled liquid region, J. Non-Cryst. Solids **352**, 3985 (2006).

[74] J. Wang, L. Wang, S. Guan, S. Zhu, R. Li, and T. Zhang, Hard rhenium–boron–cobalt amorphous alloys with a wide supercooled liquid region, Mater. Sci. Eng. A **645**, 122 (2015).

[75] M.-X. Li, S.-F. Zhoa, A. Hirata, P. Wen, H.-Y. Bai, M. Chen, J. Schroers, Y. Liu, and W.-H. Wang, High-temperature bulk metallic glasses developed by combinatorial methods, Nature **569**, 99 (2019).

[76] M. Telford, The case for bulk metallic glass, Mater. Today **7**, 36 (2004).

[77] M. Chen, A brief overview of bulk metallic glasses, NPG Asia Mater. **3**, 82 (2011).

[78] O. N. Senkov, G. B. Wilks, J. M. Scott, and D. B. Miracle, Mechanical properties of $Nb_{25}Mo_{25}Ta_{25}W_{25}$ and $V_{20}Nb_{20}Mo_{20}Ta_{20}W_{20}$ refractory high entropy alloys, Intermetallics **19**, 698 (2011).

[79] Q. Wang, J.-M. Pelletier, J. J. Blandin, and M. Suéry, Mechanical properties over the glass transition of $Zr_{41.}2Ti_{13.8}Cu_{12.5}Ni10Be_{22.5}$ bulk metallic glass, J. Non-Cryst. Solids **351**, 2224 (2005).

[80] Y. Tong, J. C. Qiao, C. Zhang, J. M. Pelletier, and Y. Yao, Mechanical properties of $Ti_{16.7}Zr_{16.7}Hf_{16.7}Cu_{16.7}Ni_{16.7}Be_{16.7}$ high-entropy bulk metallic glass, J. Non-Cryst. Solids **452**, 57 (2016).

[81] G. Y. Lai, *High Temperature Corrosion of Engineering Alloys* (American Society for Metals, Metals Park, OH, 1990).

[82] J. R. Davis, *ASM Specialty Handbook: Stainless Steels* (ASM International, Materials Park, Ohio, 1994).

[83] J. Pettersson, N. Folkeson, L.-G. Johansson, and J.-E. Svensson, The effects of KCl, K_2SO_4 and K_2CO_3 on the high temperature corrosion of a 304-type austenitic stainless steel, Oxid. Met. **76**, 93 (2011).

[84] B. A. Green, P. Liaw, and R. A. Buchanan, Corrosion behavior, in *Bulk Metallic Glasses*, edited by M. Miller and P. K. Liaw (Springer Science+Business Media, New York, 2008).

[85] A. Y. Kina, V. M. Souza, S. S. M. Tavares, J. M. Pardal, and J. A. Souza, Microstructure and intergranular corrosion resistance evaluation of AISI 304 steel for high temperature service, Mater. Charact. **59**, 651 (2008).